TÜBİTAK

Turkish Journal of Earth Sciences

http://journals.tubitak.gov.tr/earth/

Research Article

Turkish J Earth Sci
(2020) 29: 798-814

doi:10.3906/yer-2001-7

Geochemical, stable (O, C, and B) and radiogenic (Sr, Nd, Pb) isotopic data from the Eskişehir-Kızılcaören (NW-Anatolia) and the Malatya-Kuluncak (E-central Anatolia) F-REE-Th deposits, Turkey: implications for nature of carbonate-hosted mineralization

Okay ÇİMEN[1,2,*], Loretta CORCORAN[1], Corinne KUEBLER[1], Stefanie S. SIMONETTI[1], Antonio SIMONETTI[1]
[1]University of Notre Dame, Department of Civil and Environmental Engineering and Earth Sciences, South Bend, IN, USA
[2]Rare Earth Elements Application and Research Center, Munzur University, Tunceli, Turkey

Received: 06.01.2019 • **Accepted/Published Online:** 10.05.2020 • **Final Version:** 01.07.2020

Abstract: In Turkey, the largest fluorine (F)-rare earth element (REE)-thorium (Th) deposits are located within the Eskişehir-Kızılcaören (north-western Anatolia) and the Malatya-Kuluncak (east-central Anatolia) regions, and these are associated with Oligocene extensional alkaline volcanic and Late Cretecaous-Early Paleocene postcollisional intrusive rocks, respectively. In the Kızılcaören region, the basement units include the Triassic Karakaya Complex and the Late Cretaceous oceanic units (Neotethyan suture) that are cut and overlain by phonolite and carbonatite intrusions and lava flows. In the Kuluncak region, the plutonic rocks are mainly composed of syenite, quartz syenite, and rare monzonite, and these cut the late-Cretaceous Karapınar limestone, which hosts the F-REE-Th mineralization in contact zones. A carbonatite sample from the Kızılcaören region displays both a total rare earth element (TREE) concentration (4795 ppm) and $\delta^{11}B$ (–6.83‰) isotope composition consistent with mantle-derived carbonatite; whereas it is characterized by heavier $\delta^{13}C$ (+1.43‰) and $\delta^{18}O$ (+20.23‰) isotope signatures compared to those for carbonatites worldwide. In contrast, the carbonates which host the F-REE-Th mineralization in the Kuluncak region are characterized by lower TREE concentrations (5.13 to 55.88 ppm), and heavier $\delta^{13}C$ (–0.14 to –0.75‰), $\delta^{18}O$ (+27.36 to +30.61‰), and $\delta^{11}B$ (+5.38 to +6.89‰) isotope ratios compared to mantle-derived carbonatites. Moreover, the combined initial $^{87}Sr/^{86}Sr$ (0.70584 to 0.70759) and $^{143}Nd/^{144}Nd$ (0.512238 to 0.512571) isotope ratios for samples investigated here are distinct and much more radiogenic compared to those for carbonatites worldwide, and therefore indicate significant crustal input and/or hydrothermal metasomatic-related alteration. Overall, stable and radiogenic isotope data suggest that the host carbonate rocks for the F-REE-Th mineralization in both the Kızılcaören and the Kuluncak regions consist of hydrothermally metasomatized carbonatite and limestone, respectively. The mineralization in the Kızılcaören region may potentially be related to carbonatite magmatism, whereas the mineralization in the Kuluncak region, which most likely formed through interactions between the plutonic rocks and surrounding limestone at contact metamorphism zone, involved hydrothermal/magmatic fluids associated with extensive postcollisional magmatism.

Key words: Stable and radiogenic isotopes, carbonatites, metasomatised limestone, F-REE-Th mineralization in Turkey

1. Introduction

Given their unique chemical and physical characteristics, rare earth elements (REEs) are critical elements and vital components for dozens of high-tech industries including the production of solar panels, electric vehicles, computers, and smartphones (Goodenough et al., 2018). Although REE deposits occur in many geological settings and various rock types such as carbonatites, hydrothermal deposits, alkaline to peralkaline igneous rocks, weathered ion adsorption clay deposits, and heavy mineral placers (e.g., Chakhmouradian and Wall, 2012; Kynicky et al., 2012; Jaireth et al., 2014; Nikiforov et al., 2014; Goodenough et al., 2018; Öztürk et al., 2019a; Zheng and Lui, 2019), they are mainly mined from two mineral-deposit types in China (Verplank, 2017), which are carbonatite-related (e.g., Bayan Obo; Zhang et al., 2017; Chen et al., 2019) and ion adsorption clay deposits (e.g., Yang et al., 2013; Fu et al., 2019). Therefore, carbonatites are significant target rocks for REE exploration activities and are associated with unique chemical and mineralogical characteristics that include high concentrations of Nd and Sr (e.g., Bell and Simonetti, 2010), and >50 % of carbonate minerals (Wooley and Kempe, 1989).

Carbonatites may form in different tectonic settings (Woolley, 1989) including continental rifts (e.g., East African; Simonetti and Bell, 1993), and oceanic plates (e.g., Cape Verde Islands; Hoernle et al., 2002; Kogarko et al., 2009), and orogenic belts (e.g., British Columbia,

* Correspondence: okaycimen@gmail.com

western Canada, and Miaoya Complex, central China; Millonig et al., 2012; Mitchell et al., 2017; Çimen et al., 2018, 2019). In Europe, the main REE metallogenetic provinces include the Gardar Province of south-west Greenland, the Protogine Zone in southern Sweden, the Kola Alkaline Province, and the Oslo Rift in Norway that are associated with alkaline silicate and carbonatite magmatism, and most likely occurred within extensional tectonic settings (Goodenough et al., 2018). Apart from the intracontinental rift zones, potential REE deposits may also form by magmatic and hydrothermal activity in orogenic belts (e.g., Loch Loyal Syenite Complex, Caledonides; Walters et al., 2013; Goodenough et al., 2018). REEs may also be concentrated by hydrothermal processes based on theoretical and experimental studies (Williams-Jones et al., 2012; Li and Zhou, 2018). Hydrothermal processes are mainly associated with carbonatites and peralkaline silicate rocks and include REE abundances at the weight percent concentration levels (Williams-Jones et al., 2012). There are several REE deposits worldwide, which may have formed as a result of coupled magmatic and hydrothermal processes (e.g., Sin Quyen Deposit, Northwestern Vietnam, Li and Zhou, 2018; the Nechalacho deposit, Northwest Territories, Canada; and the Strange Lake deposit in Québec-Labrador, Canada; Williams-Jones et al., 2012 and references therein).

A section of the Alpine–Himalayan orogenic belt is located in Turkey, which formed by the agglomeration of several terranes or continental micro-plates (e.g., İstanbul Zonguldak, Sakarya and Anatolide Tauride) during the closure of different branches of the Tethyan Ocean (e.g., Şengör and Yılmaz, 1981; Göncüoğlu et al., 1997). Although there are significant occurrences of REE mineralizations in Turkey (e.g., Eskişehir-Kızılcaören, Malatya-Kuluncak, Sivas-Karaçayır), there is still no consensus on the petrogenesis of the mineralization in these regions due to the limited number of previous studies and scarcity of geochemical and radiogenic and stable isotope data. Based on a report (in Turkish) published by the General Directorate of Mineral Research and Explorations (MTA) in 2017, the Kızılcaören deposit has ~4 million tons of REEs with an average grade of ~3% among these deposits. Thus, it is clear that Turkey has enough REE deposits to establish a secured and uninterrupted supply of REEs, which are critical for burgeoning high-tech activities. However, the geological and mineralogical characteristics of these REE deposits must be fully understood and investigated since beneficiation methods are specifically developed for each deposit, and based on properties including mineralogy, grain size and textures (Jordens et al., 2013; Goodenough et al., 2018). Therefore, for the first time, this study reports combined trace element, stable (B, C, and O) and radiogenic (Nd, Pb, and Sr) isotope data from the Eskişehir-Kızılcaören and the Malatya-Kuluncak deposits in order to investigate possible links to carbonatite magmatism and decipher the sources of the ore-forming melts/fluids.

2. Geological setting

2.1. Eskişehir-Kızılcaören deposit, northwestern Turkey

The Eskişehir-Kızılcaören deposit is located in northwestern Turkey and includes fluorite-bastnäsite-barite mineralization (Figure 1). The mineralization has been reported as ~4.67 Mt of REEs (Ce+La+Nd+Y) at an average grade of 2.78 wt% (Kaplan, 1977; Öztürk et al., 2019a), which represents the most significant REE-type deposit in Turkey. This deposit was found in 1959 conducting aerial gamma-ray spectrometry due to Th-based radioactivity (Gültekin et al., 2003). It is located north of İzmir-Ankara-Erzincan Suture Belt (IAESB) and within the Karakaya Complex of the Sakarya Composite Terrane (SCT; Okay and Göncüoğlu, 2004), which includes mostly crustal rocks (e.g., Sayit and Göncüoğlu, 2009), and accretionary units of the Paleotethyan Ocean (e.g., Çimen et al., 2017). The Triassic Karakaya Complex, which consists of deformed and metamorphosed volcanic and clastic units (Okay and Göncüoğlu, 2004), is tectonically thrusted over by oceanic fragments of the IAESB. The Triassic clastic sequence of the upper Karakaya Complex in the mineralization area (Figure 2A) is mostly composed of metagreywacke and metaarkose, and a lesser amount of mudstone/shale interbeds, and limestone blocks (Gültekin et al., 2003).

The Karakaya Complex and oceanic crust fragments (serpentinized ultramafic rocks) are cut and overlain by alkaline magmatic rocks such as phonolite, trachyte, sporadic dike-shaped bodies of carbonatites and carbonate–silicate rocks, and stockwork zones of bastnaesite–barite–fluorite ore (Figure 2A; e.g., Gültekin et al., 2003; Sarıfakıoğlu et al., 2009; Nikiforov et al., 2014). The alkaline silicate rocks, phonolite (about 500 m in diameter) and trachyte, outcrop in the south of mineralized area and cut the ophiolitic rocks (Nikiforov et al., 2014). The phonolites are partly altered light pinkish-grey and composed of sanidine, clinopyroxene, feldspathoid, analcime, and volcanic glass (for detailed mineralogy of phonolite and trachyte, see Sarıfakıoğlu et al., 2009). Carbonatites and carbonate–silicate rocks form irregularly shaped bodies within zones of tectonic breccias, whereas the mineralization is composed of porous medium- to coarse-grained bastnaesite-barite-fluorite-rich veins in localized crush zones or tectonic and volcanic (?) breccia (for detailed field descriptions and mineralogy, see Nikiforov et al., 2014). The remaining associated minerals are calcite, quartz, psilomelane,

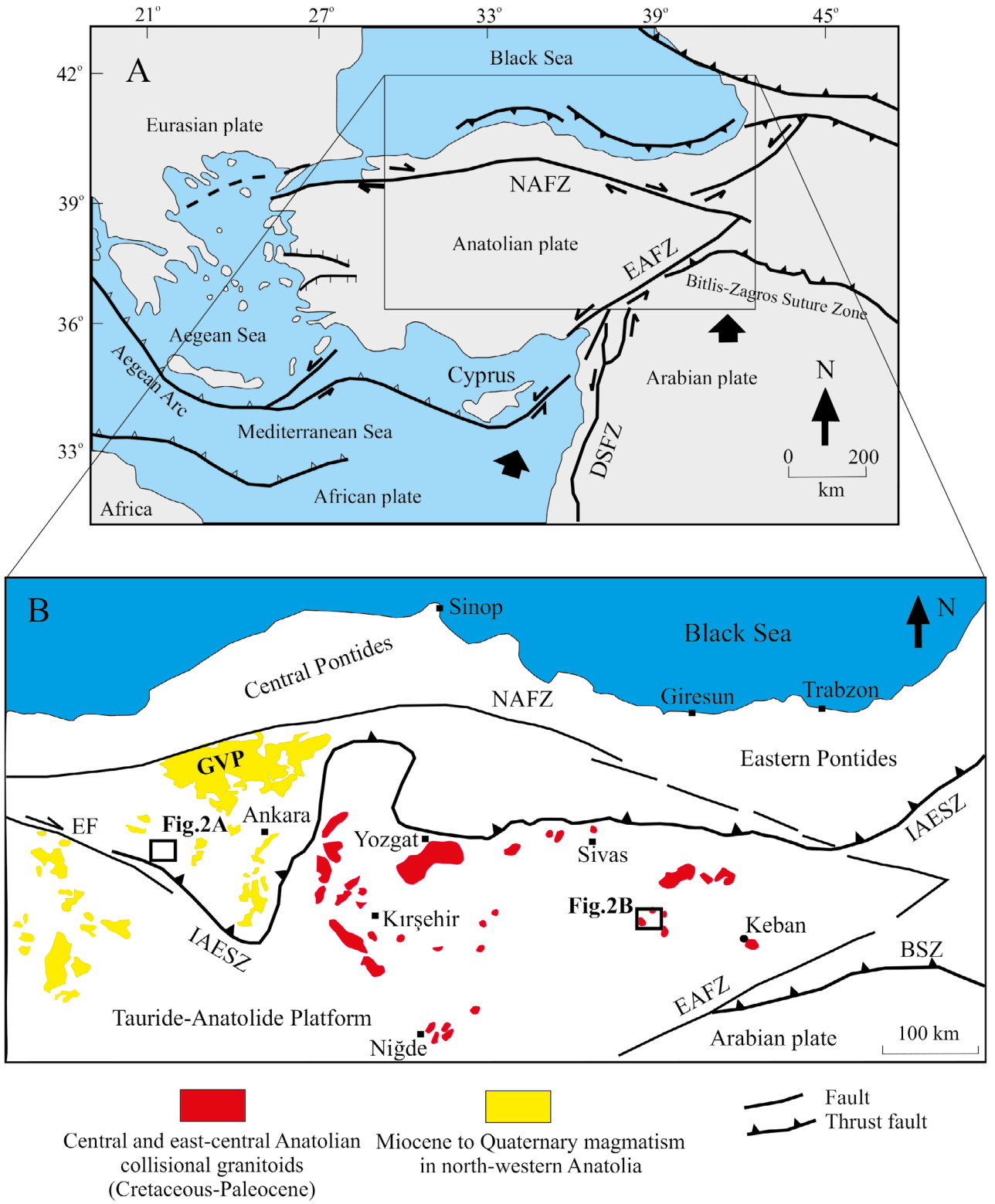

Figure 1. (**A**) Tectonic map of Turkey (modified from Boztuğ et al., 2007), and (**B**) Distribution of the Miocene to Quaternary magmatism in north-western Turkey (modified from Ersoy et al., 2012), and Createcous-Paleocene collisional granitoids in east-central Turkey (modified from Boztuğ et al., 2007). NAFZ: North Anatolian Fault Zone, EAFZ: East Anatolian Fault Zone, DSFZ: Dead Sea Fault Zone, IAESZ: Izmir-Ankara-Erzincan Suture Zone, GVP: Galatia Volcanic Province, BSZ: Bitlis-Zagros Suture Zone.

pyrolusite, goethite, pyrite, hematite, braunite, plagioclase feldspar, rutile, and phlogopite (Gültekin et al., 2003). The thicknesses of carbonatite dikes vary between 1.0 and 1.5 m (Özgenç, 1993). It must be noted that Ersoy et al. (2018) reported the presence of carbonatite lava flows in the field. Also, the alkaline metasomatism (e.g., fenitization) in the host rocks of the carbonatites has been reported by Öztürk et al. (2019a). Radiometric age dating results obtained from sanidine phenocrysts (Ar/Ar method) in phonolite and phlogopite crystals (K-Ar method) in carbonatite indicate that the alkaline magmatism occurred in the late Oligocene-early Miocene time (around 24-25 Ma; Sarıfakıoğlu et al., 2009; Nikiforov et al., 2014).

2.2. Malatya Kuluncak deposit, east-central Turkey

The Malatya-Kuluncak deposit is located in east-central Turkey and associated with the late Cretaceous-early Paleocene postcollisional intrusive rocks (Figure 1). In this region, the postcollisional intrusive rocks (Hasançelebi, Başören-Malatya) are situated in the Eastern Tauride Platform (Özgenç and İlbeyli, 2009), and may belong to the Central Anatolian collisional granitoids (Figure 1; Boztuğ et al., 2007, 2009). In the study area, the upper Cretaceous–lower Paleocene Karapınar limestone and Kızılkaya ophiolitic rocks represent the basement (Figure 2B; Özgenç and İlbeyli, 2009). The Başören plutonic rocks form as small stocks and are mainly composed of syenite, quartz syenite, and rare monzonite, and cut by pegmatitic, mafic, and aplitic dykes (Özgenç and İlbeyli, 2009). The late-Cretaceous Karapınar limestone is intruded by these stocks and hosts the F-REE-Th mineralization that formed in contact zones (Figure 2B). Leo et al. (1974) reported an early Paleocene age data (K-Ar; 65 Ma) from an alkaline syenite in the Başören region, whereas Boztuğ et al. (2009) published Ar-Ar ages of 72 and 77 Ma from the Kuluncak Pluton. In addition, these rocks are overlain by a middle-upper Miocene volcanic and sedimentary sequence, which includes mostly pyroclastic units, olivine-phyric basalts and andesitic lavas (Özgenç and İlbeyli, 2009). The radiometric ages from the volcanic rocks, which include basalt, andesite, and dacite range between 14 and 19 Ma (Leo et al., 1974). Özgenç and Kibici (1994) and Özgenç and İlbeyli (2009) defined carbonatite-hosted fluorite deposits in the region and the term "carbonatite-associated" has also been adopted by recently published studies (Öztürk et al., 2019a, b). Özgenç and İlbeyli (2009) suggested that carbonatite (as ring dykes) could have formed as a result of the last stage intrusive activity that caused the fenitization (up to 200 m wide) of the syenites, and formation of small quantities of britholite (contains 57% REE) and fluorite. Here, the other associated mineral phases are bastnäsite, apatite, siderite, calcite, and quartz (Öztürk et al., 2019a). It should be noted that Leo et al. (1974) did not observe any field evidence for carbonatite occurrences.

3. Mineralogical and textural characteristics

In the Kızılcaören deposit, the carbonatite is composed of mostly fine-grained calcite and includes a minor amount of barite, phlogopite, and Fe-Mn hydroxides (Figures 3A and 3B). In the samples investigated here, the phenocrysts are represented by phlogopite, barite, and Fe-Mn hydroxides

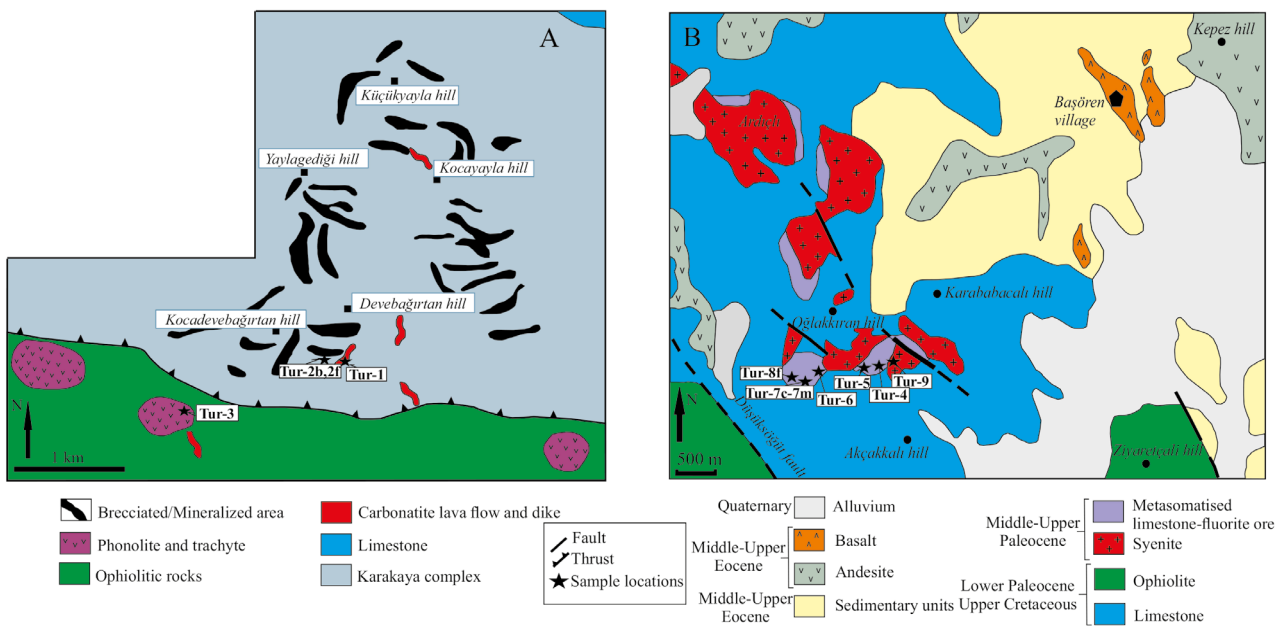

Figure 2. Geological maps of the **(A)** Eskişehir-Kızılcaören region (modified after Nikiforov et al., 2014) and **(B)** the Malatya-Kuluncak region (modified after Özgenç and İlbeyli, 2009).

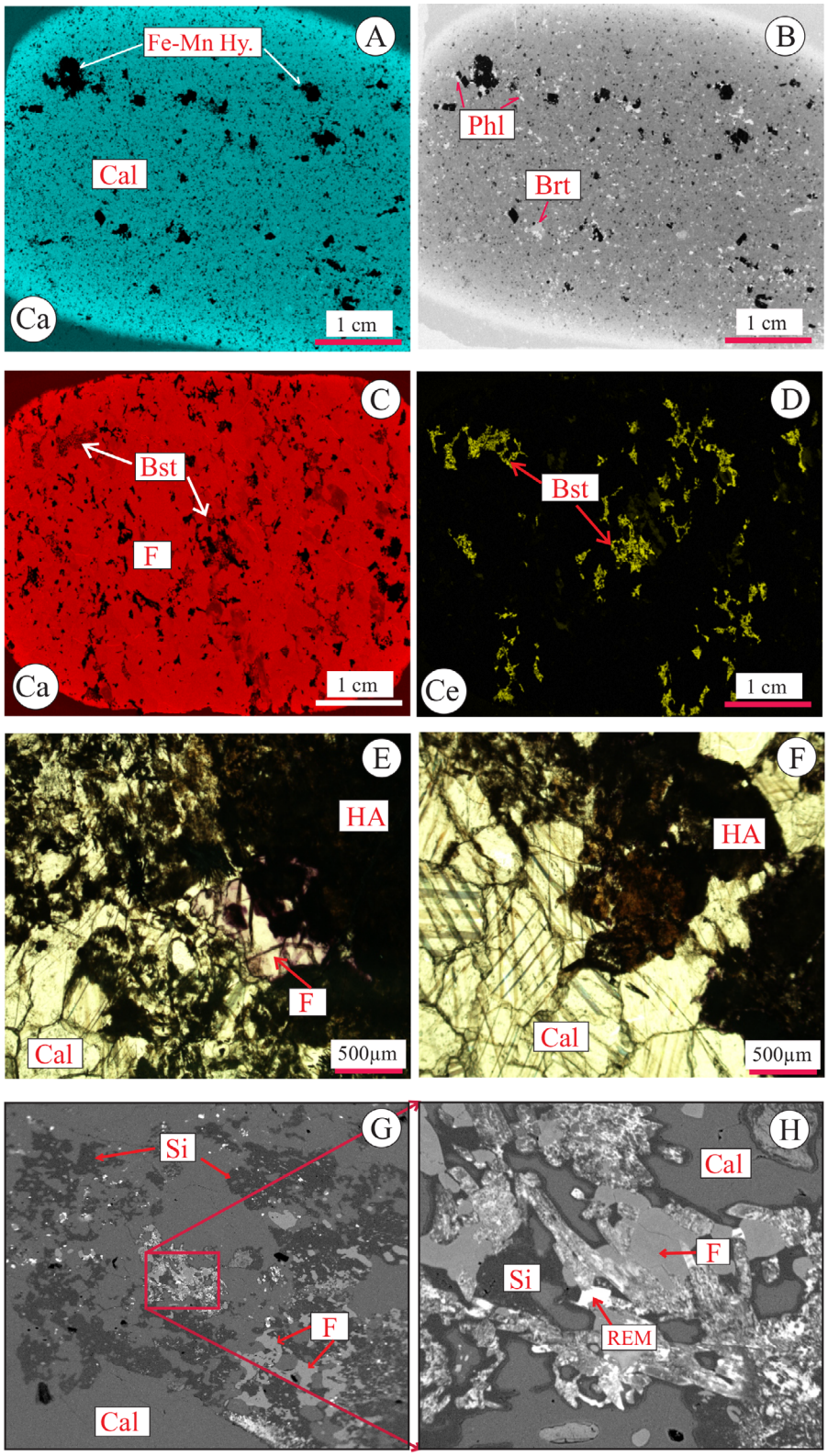

Figure 3. Micro-XRF images for carbonatite **(A, B)** and fluorite-bastnaesite **(C, D)** samples from the Eskişehir-Kızılcaören deposit, and thin section **(E, F)** and back scatter electron **(G, H)** images for a mineralized vein from the Malatya-Kuluncak deposit. Cal: Calcite, Fe-Mn Hy: Iron and manganese (hydr)oxides, Phl: Phlogopite, Brt: Barite, F: Fluorite, Bst: Bastnaesite, HA: Hydrothermally Altered Si: Silica, REM: Rare Earth Mineral.

in a calcite matrix and are characterized by subhedral to euhedral shapes. Moreover, minor and accessory phases of apatite, pyrochlore, and parisite have been identified in carbonatite samples (Nikiforov et al., 2014). The fluorite-bearing sample (Tur-2f) is characterized by its purple color and contains a significant amount of Ce- bastnaesite and barite crystals, which have anhedral to subhedral shapes (Figures 3C and 3D). The phonolite displays porphyritic texture and the phenocrysts are characterized by feldspar and pyroxene crystals set within a fine-grained matrix. Gültekin et al. (2003) and Nikiforov et al. (2014) report the detailed mineralogy of the silicate rocks, carbonatites, and ore mineralization within the Kızılcaören deposit. The carbonate rocks of the Kuluncak deposit are composed of medium- to coarse-grained calcite, which show well-defined rhombohedral crystal outlines (Figures 3E and 3F). These calcite crystals have been impacted by hydrothermal alteration, which resulted in the crystallization of Si-phases, fluorites, rare earth minerals, Th-rich phases, and Mn hydroxides (Figures 3G and 3H). In addition, secondary Mn-veins cut the carbonate rocks in the field. The syenite exhibits porphyritic texture and consists predominantly of K-feldspar, clinopyroxene, phlogopite, and feldspathoid (for detailed mineralogy, see Leo et al., 1978).

4. Analytical methods

The semiquantitative chemical maps illustrated in Figure 3 were procured using an Edax Orbis µ-XRF instrument at the Center for Environmental Science and Technology (CEST), University of Notre Dame. The operational conditions for the instrument: amplifier time of 12.8 µs, fluorescent energy of 32 kV, and beam size of 30 µm. The mineral identification and back-scattered electron (BSE) images were performed by a CAMECA SX-50 electron microprobe (EMP) at the same university. The EMP instrument conducted with an accelerating voltage of 15kV, 10nA of beam current, and 15 µm of beam diameter. Calcite, fluorite, bastnaesite, and manganese separates were obtained from the samples by hand-picking using a binocular microscope. Trace element concentrations (Table 1) were obtained via solution (wet plasma)-mode analysis performing a Nu Plasma AttoM (high resolution) HR-ICP-MS instrument.

The $\delta^{18}O$ and $\delta^{13}C$ isotope data for carbonate and bastnaesite separates reported in this study (Table 2) were procured using a Delta V Advantage isotope ratio mass spectrometer at CEST. B, Sr, Nd, and Pb isotope ratio measurements (Tables 3 and 4) were determined via solution-mode on a Nu Plasma- II multi-collector-ICP-MS housed within Midwest Isotope and Trace Element Research Center, University of Notre Dame. Çimen et al. (2018, 2019) reports detailed information in relation to the analytical procedures employed in this study for the determination of trace element abundances, and stable and radiogenic isotope analyses.

5. Results

5.1. Trace element geochemistry

Trace element concentrations for samples from the Eskişehir-Kızılcaören and the Malatya-Kuluncak deposits are reported in Table 1. The chondrite-normalized (CN)-REE pattern for carbonatite sample (Tur-1) from the Kızılcaören deposit ($La/Lu_{(CN)}$ = 137.08; Table 1) displays a distinct enrichment in LREEs over HREEs, which is similar to those for carbonatites worldwide (Figure 4A). In contrast, the carbonate separates for samples Tur-4, Tur-5, Tur-6, and Tur-7c from the Kuluncak deposit show similar enrichment in LREEs over HREEs ($La/Lu_{(CN)}$ = 19.18–320.06) coupled with slight negative Eu anomalies (Eu/Eu^*=0.57–0.76; $2Eu_{CN}/[(Sm_{CN} + Gd_{CN})]$); these LREE enrichment levels and TREE contents (5.13 to 55.88 ppm) are much lower than those for typical carbonatites worldwide (Figure 4B). Apart from the carbonate rocks, the bastnasite (Tur-2b), fluorite (Tur-2f), and phonolite (Tur-3) samples from the Kızılcaören deposit exhibit similarly sloped CN-REE patterns, but plot at different LREE enrichment levels over HREEs (Figure 4C). For the Kuluncak deposit, the fluorite (Tur-8f) and syenite (Tur-9) samples show similar CN-REE patterns (enrichment in LREEs over HREEs) coupled with slight negative Eu anomalies; in contrast, the Mn-rich sample (Tur-7m) displays enrichments in LREEs and HREEs over middle REEs (Figure 4D). The B content is ≤ 1 ppm (Table 1, 0.36 ppm) for the carbonatite sample from the Kızılcaören deposit, which is consistent with those for asthenosphere-derived, mid-ocean ridge basalts (e.g., MORBs; Spivack and Edmond, 1987; Wunder et al. 2005; Marschall et al., 2017), and mantle-derived carbonatites (Hulett et al., 2016; Çimen et al., 2018, 2019). However, the carbonate rocks from the Kuluncak deposit clearly have higher B contents (ranging from 1.57 to 7.54 ppm; Table 1) than those from fresh MORBs and typical for carbonatites worldwide.

5.2. Stable isotope signatures

Oxygen and carbon stable isotope data for carbonatite (Tur-1), bastnasite (Tur-2b), and carbonate (Tur-4, 5, 6, 7c) rock samples from the Kızılcaören and Kuluncak deposits are listed in Table 2. The $\delta^{18}O_{SMOW}$ (‰) and $\delta^{13}C_{PDB}$ (‰) values change between +20.23 ‰ and +30.61 ‰, and –3.56 ‰ and +1.43 ‰, respectively, and plot outside and to the right of the field for "primary igneous carbonatites (PIC)" (Keller and Hoefs, 1995; Figure 5). The $\delta^{11}B$ (‰) value for the carbonatite sample from the Kızılcaören deposit is –6.83 ±0.5 ‰ and overlaps (given its associated uncertainty) with value for asthenospheric mantle (approximately –7.1 ±0.9 ‰; Marschall et al., 2017). In contrast, the $\delta^{11}B$ signatures (+5.38 ‰ to +6.89

Table 1. Trace element concentrations (ppm) for samples from the Eskişehir-Kızılcaören and Malatya Kuluncak deposits.

	Eskişehir-Kızılcaören deposit				*Malatya Kuluncak deposit*						
Sample	Tur-1	Tur-2b	Tur-2f	Tur-3	Tur-4	Tur-5	Tur-6	Tur-7c	Tur-7m	Tur-8f	Tur-9
Sc	1.24	0.48	0.12	0.24	0.08	0.16	0.10	0.07	0.01	0.01	0.02
V	37.2	10.3	7.78	7.26	0.42	0.33	0.31	0.48	1.05	0.23	0.19
Cr	0.27	0.15	b.d.	0.76	0.16	0.12	0.07	0.04	b.d.	0.21	0.15
Co	0.38	b.d.	0.06	0.10	0.17	0.17	0.15	0.14	0.10	0.02	0.01
Ni	2.52	0.37	0.63	0.68	3.23	2.92	3.12	3.09	0.53	0.96	0.96
Cu	0.91	3.10	2.19	0.40	0.60	1.07	0.85	0.55	0.71	0.67	0.21
Zn	170	47.1	25.4	48.3	8.71	26.7	5.77	15.4	14.1	13.4	36.0
Rb	1.21	0.10	0.06	15.05	0.58	0.37	0.71	0.19	0.23	13.4	30.8
Sr	335	353	394	119	199	187	266	192	15.6	168	17.9
Y	45.3	51.1	16.68	2.53	2.06	1.23	2.09	1.29	4.22	36.9	9.17
Zr	4.13	5.58	3.21	2147	0.53	0.54	0.24	0.29	0.74	3.78	13.5
Nb	44.7	3.51	6.41	23.0	0.32	0.17	0.35	0.15	0.34	4.82	12.5
Mo	3.23	2.17	6.74	0.12	0.81	1.84	0.42	0.34	0.61	0.08	0.07
Cs	0.07	0.01	0.01	2.05	0.06	0.03	0.08	0.02	0.01	0.34	7.33
Ba	589	3089	8073	222	10.4	7.3	27.2	21.7	16.5	4.69	32.3
La	840	60212	233	46.6	2.82	1.50	26.9	3.33	1.28	176	36.0
Ce	27831	7661	710	49.7	2.35	2.22	23.4	3.24	1.88	454	57.9
Pr	246	1216	21.1	3.78	0.22	0.18	1.32	0.24	0.18	30.9	5.16
Nd	753	1808	44.4	10.7	0.68	0.67	3.14	0.73	0.61	75.5	15.8
Sm	89.9	39.0	2.45	1.14	0.11	0.11	0.33	0.10	0.10	6.99	2.14
Eu	17.5	5.59	0.41	0.27	0.02	0.03	0.07	0.02	0.02	1.14	0.42
Gd	35.6	16.11	1.78	0.63	0.13	0.10	0.27	0.10	0.12	4.52	1.81
Tb	2.99	1.24	0.15	0.08	0.02	0.02	0.04	0.02	0.02	0.54	0.29
Dy	12.1	7.41	0.88	0.43	0.16	0.12	0.20	0.10	0.26	2.81	1.76
Ho	2.08	1.86	0.22	0.09	0.04	0.03	0.05	0.02	0.08	0.58	0.40
Er	5.00	5.61	0.72	0.24	0.12	0.08	0.14	0.07	0.33	1.34	0.91
Tm	0.70	0.87	0.11	0.04	0.01	0.01	0.02	0.01	0.06	0.13	0.11
Yb	4.77	5.40	0.82	0.31	0.09	0.05	0.09	0.04	0.31	0.55	0.49
Lu	0.66	0.75	0.12	0.04	0.01	0.01	0.01	0.01	0.03	0.04	0.04
Hf	0.04	0.06	0.03	2.23	0.01	0.01	0.01	0.00	0.01	0.03	0.19
Pb	242	12.3	14.0	24.5	119	46.7	23.9	1.81	10.9	11.2	6.86
Th	41.3	212	20.4	29.2	0.17	0.32	0.21	0.27	0.09	2.16	10.80
U	14.6	86.7	3.56	11.04	0.47	0.89	0.37	0.92	0.53	0.21	5.08
B	0.36	n.a.	n.a.	n.a.	2.29	2.21	7.4	1.57	n.a.	n.a.	n.a.

Note: b.d.=below detection limit; n.a.=not analyzed

‰) of carbonate rocks from the Kuluncak deposit yield much higher values than typical MORB mantle, and plot outside of the field defined by pristine, mantle-derived carbonatites worldwide (Figure 6; Hulett et al., 2016; Çimen et al., 2018, 2019).

5.3. Radiogenic isotope characteristics

The Sr, Nd, and Pb isotope data for carbonate separates and silicate rocks from the Eskişehir-Kızılcaören and Malatya-Kuluncak deposits are listed in Tables 3 and 4, and shown in Figures 6–8. The ages of 25 Ma (for the Kızılcaören

Table 2. C, O, and B isotope data for carbonate samples from the Eskişehir-Kızılcaören and Malatya Kuluncak deposits.

Sample	$\delta^{13}C$ (‰)	uncertainty	$\delta^{18}O$ (‰)	uncertainty	$\delta^{11}B$ (‰) *
Tur-1	1.43	0.04	20.23	0.05	–6.83
Tur-2b	–3.56	0.39	20.94	0.83	n.a.
Tur-4	–0.75	0.03	29.71	0.04	5.86
Tur-5	–0.63	0.03	30.61	0.05	5.38
Tur-6	–0.64	0.06	27.36	0.04	6.89
Tur-7c	–0.14	0.02	29.15	0.03	6.72

*: Uncertainty associated with B isotope ratios is ±0.5‰ (2s level) based on replicate analyses of coral in-house standard (see text for details). n.a.=not analyzed

Table 3. Sr and Nd isotope data for samples from the Eskişehir-Kızılcaören and Malatya Kuluncak deposits.

Sample	Rb (ppm)	Sr (ppm)	$^{87}Rb/^{86}Sr$	$^{87}Sr/^{86}Sr$	2σ	$^{87}Sr/^{86}Sr$ *(i)*	Sm (ppm)	Nd (ppm)	$^{147}Sm/^{144}Nd$	$^{143}Nd/^{144}Nd$	2σ	$^{143}Nd/^{144}Nd$ *(i)*	ƐNd *(t)*
Tur-1	1.21	334	0.0105	0.70605	0.00001	0.70605	89.9	753	0.072	0.51256	0.00001	0.51255	–1.1
Tur-2b	0.10	353	0.0008	0.70596	0.00002	0.70596	39.0	1808	0.013	0.51257	0.00001	0.51257	–0.8
Tur-2f	0.06	393	0.0004	0.70584	0.00001	0.70584	2.45	44.4	0.033	0.51258	0.00001	0.51257	–0.7
Tur-3	15.1	119	0.365	0.70649	0.00001	0.70636	1.14	10.7	0.064	0.51256	0.00001	0.51255	–1.2
Tur-4	0.58	199	0.0084	0.70742	0.00001	0.70741	0.11	0.68	0.097	0.51248	0.00001	0.51244	–2.3
Tur-5	0.37	186	0.0057	0.70752	0.00001	0.70752	0.11	0.67	0.099	0.51228	0.00001	0.51224	–6.2
Tur-6	0.71	266	0.0077	0.70746	0.00001	0.70746	0.33	3.14	0.063	0.51248	0.00001	0.51245	–2
Tur-7c	0.19	191	0.0036	0.70759	0.00001	0.70759	0.10	0.73	0.082	0.51245	0.00001	0.51241	–2.7
Tur-7m	0.23	15.6	0.0428	0.70792	0.00001	0.70788	0.10	0.61	0.099	0.51257	0.00001	0.51253	–0.5
Tur-8f	13.4	168	0.230	0.70803	0.00001	0.70782	6.99	75.5	0.056	0.51250	0.00001	0.51248	–1.6
Tur-9	30.8	17.9	4.985	0.71181	0.00001	0.70720	2.14	15.8	0.081	0.51253	0.00001	0.51249	–1.2

Please see the text for age correction. $^{87}Rb/^{86}Sr$ and $^{147}Sm/^{144}Nd$ values were calculated based on ICP-MS-determined elemental abundances and are associated with relative uncertainties of between 3% and 5% (2s level).

deposit; Delaloye and Özgenç, 1983; Sarıfakıoğlu et al., 2009; Nikiforov et al., 2014) and 65 Ma (for the Kuluncak deposit; Leo et al., 1974) have been adopted for the age corrections of the measured Sr, Nd, and Pb isotope ratios. The magnitude of the age correction of the measured $^{87}Sr/^{86}Sr$ ratios (0.70584 to 0.70803; Table 3) is minimal due to the low $^{87}Rb/^{86}Sr$ values (0 to 0.365) and relatively young ages of both complexes with exception of the syenite sample ($^{87}Rb/^{86}Sr$= 4.985) from the Kuluncak deposit. While the $Sr_{(i)}$ isotope values for samples from the Kızılcaören deposit are tightly constrained between 0.70584 and 0.70586, the samples from the Kuluncak deposit show slightly more radiogenic $Sr_{(i)}$ isotope values (0.70720 to 0.70788). The $^{143}Nd/^{144}Nd_{(i)}$ ratios vary between 0.51224 and 0.51257 for all samples based upon the low $^{147}Sm/^{144}Nd$ ratios (~0.013 to ~0.099; Table 3). The $^{143}Nd/^{144}Nd_{(i)}$ isotope ratios (0.51255 to 0.51257) for samples from the Kızılcaören deposit yield $Ɛ_{Nd\ (25Ma)}$ values of –0.7 to –1.2 (Table 3, Figure 7A). In the Kuluncak deposit, Tur-5 sample is characterized by a lower initial $^{143}Nd/^{144}Nd$ value (0.51224) than the remaining samples (0.51241 to 0.51253), and the corresponding $Ɛ_{Nd\ (65Ma)}$ values for all samples vary between –0.5 and –6.2 (Table 3, Figure 7A). All samples from the Kızılcaören and Kuluncak deposits define a fairly restricted range of $^{206}Pb/^{204}Pb$ (18.85 to 19.42), $^{207}Pb/^{204}Pb$ (15.70 to 15.77), and $^{208}Pb/^{204}Pb$ (39.09 to 39.83) ratios (Table 4; Figure 7B). Moreover, Tur-2b sample (bastnasite) is characterized by higher $^{206}Pb/^{204}Pb$ and $^{208}Pb/^{204}Pb$ ratios compared to the other samples, whereas Tur-7c sample (hydrothermally metasomatized limestone) has slightly higher $^{206}Pb/^{204}Pb$ ratio than rest of the samples (Figure 8). Since the U/Pb ratios are very small (0.04–0.746), except for Tur-2b

Table 4. Pb isotope data for samples from the Eskişehir-Kızılcaören and Malatya Kuluncak deposits.

Sample	U (ppm)	Pb (ppm)	Th (ppm)	$^{238}U/^{204}Pb$	$^{235}U/^{204}Pb$	$^{232}Th/^{204}Pb$	$^{206}Pb/^{204}Pb$	2σ	$^{207}Pb/^{204}Pb$	2σ	$^{208}Pb/^{204}Pb$	2σ
Tur-1	14.6	242	41.3	3.87	0.03	11.3	18.851	0.0010	15.698	0.0008	39.089	0.0023
Tur-2b	86.7	12.3	212	465	3.32	1178	19.922	0.0110	15.768	0.0087	39.826	0.0218
Tur-2f	3.56	14.0	20.4	16.5	0.12	97.7	19.104	0.0010	15.720	0.0010	39.378	0.0024
Tur-3	11.0	24.5	29.2	29.2	0.21	79.6	18.975	0.0006	15.734	0.0005	39.233	0.0013
Tur-4	0.47	119	0.17	0.25	0.002	0.10	18.971	0.0006	15.716	0.0005	39.116	0.0014
Tur-5	0.89	46.7	0.32	1.23	0.01	0.46	18.983	0.0012	15.715	0.0006	39.082	0.0016
Tur-6	0.37	23.9	0.21	1.01	0.01	0.60	19.029	0.0010	15.713	0.0009	39.061	0.0025
Tur-7c	0.92	1.81	0.27	33.2	0.24	9.95	19.749	0.0012	15.746	0.0010	39.095	0.0027
Tur-7m	0.53	10.9	0.09	3.17	0.02	0.53	19.071	0.0005	15.719	0.0004	39.114	0.0010
Tur-8f	0.21	11.2	2.16	1.22	0.01	12.9	18.955	0.0007	15.708	0.0006	39.212	0.0016
Tur-9	5.08	6.79	10.8	48.9	0.35	107	19.492	0.0010	15.733	0.0009	39.430	0.0023

Table 4. Pb isotope data for samples from the Eskişehir-Kızılcaören and Malatya Kuluncak deposits (continued).

Sample	$^{207}Pb/^{206}Pb$	2σ	$^{208}Pb/^{206}Pb$	2σ	$^{206}Pb/^{204}Pb$ *(i)*	$^{207}Pb/^{204}Pb$ *(i)*	$^{208}Pb/^{204}Pb$ *(i)*
Tur-1	0.83	0.00002	2.07	0.00006	18.84	15.70	39.07
Tur-2b	0.79	0.00004	2.00	0.00008	18.11	15.69	38.37
Tur-2f	0.82	0.00001	2.06	0.00005	19.04	15.72	39.26
Tur-3	0.83	0.00001	2.07	0.00003	18.86	15.73	39.13
Tur-4	0.83	0.00001	2.06	0.00003	18.97	15.72	39.12
Tur-5	0.83	0.00005	2.06	0.00015	18.97	15.71	39.08
Tur-6	0.83	0.00001	2.05	0.00004	19.02	15.71	39.06
Tur-7c	0.80	0.00001	1.98	0.00004	19.41	15.73	39.06
Tur-7m	0.82	0.00001	2.05	0.00003	19.04	15.72	39.11
Tur-8f	0.83	0.00001	2.07	0.00003	18.94	15.71	39.17
Tur-9	0.81	0.00002	2.02	0.00003	19.00	15.71	39.08

(7.047); therefore, the age correction for the Pb isotopic ratios is minimal (Table 4).

6. Discussion

6.1. Origin of carbonate host rocks

As stated earlier, mantle-derived carbonatites contain high abundances of REEs, Sr, and volatiles (e.g., Jones et al., 2013), in particular, their TREE contents are distinctly higher than those for sedimentary carbonate (<200 ppm; e.g., Xu et al., 2010). The carbonatite sample from the Kızılcaören deposit displays a similar CN-REE pattern and enrichment level compared with worldwide carbonatite occurrences (Figure 4A), whereas the carbonate rocks from the Kuluncak deposit have much lower TREE contents (Figure 4B). Moreover, the B concentration of the carbonatite sample from the Kızılcaören deposit is consistent with those of fresh MORBs (Spivack and Edmond, 1987; Wunder et al., 2005) and most of igneous carbonatites (Hulett et al., 2016; Çimen et al., 2018, 2019), whereas the carbonate rocks from the Kuluncak deposit clearly have higher B contents (Table 1); this result is consistent with greater crustal involvement/contamination due to the overall higher concentration of an incompatible element such as B in crustal rocks (Marschall et al., 2017). Overall, the trace element data reported here indicate the presence of a significant sedimentary component to the carbonate for the Kuluncak deposit rather than mantle-derived calcite.

The $\delta^{18}O_{SMOW}$ (‰) and $\delta^{13}C_{PDB}$ (‰) signatures of igneous carbonates are commonly used as reliable tracers

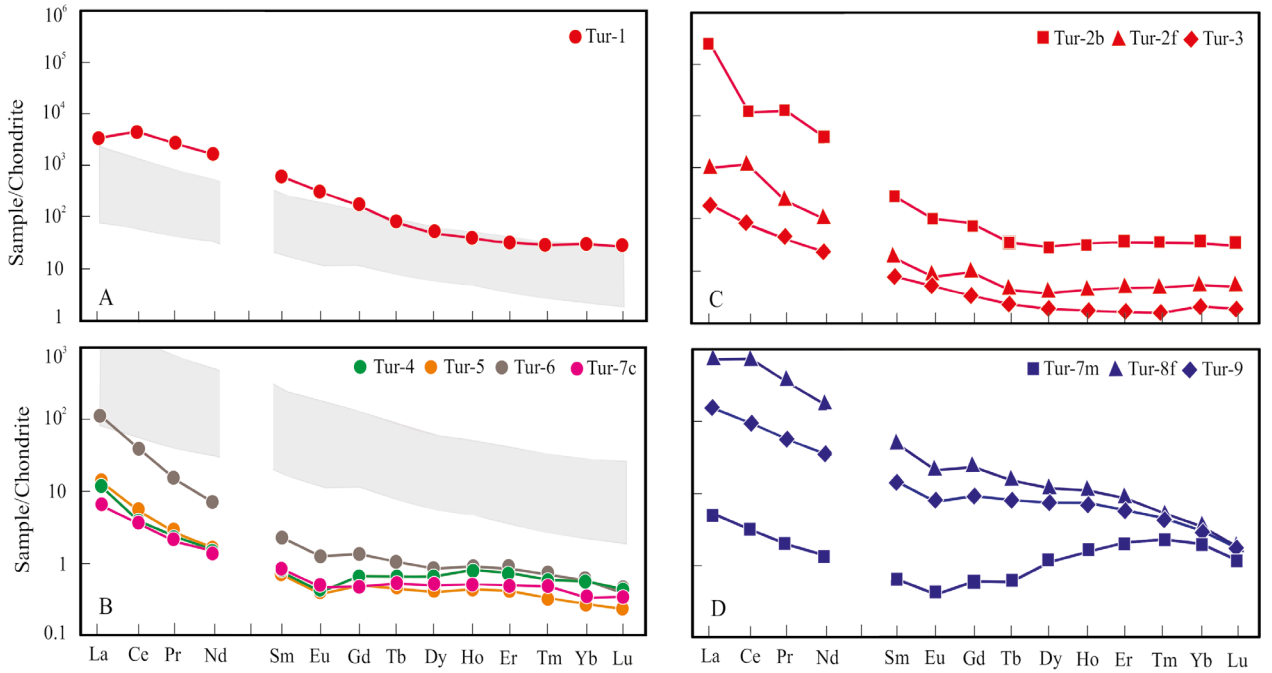

Figure 4. Chondrite-normalized rare earth element patterns for samples from the Eskişehir-Kızılcaören **(A, C)** and the Malatya-Kuluncak **(B, D)** deposits. Chondrite values are from McDonough and Sun (1995). The gray field represents data for carbonate separates from the Miaoya complex (Central China, Çimen et al., 2018), and Blue River (British Columbia, Canada), Chipman Lake Carbonatite (Ontario,Canada), Jacupiranga (São Paulo State, Brazil) and Fen complex (Telemark, Norway) regions (Çimen et al., 2019).

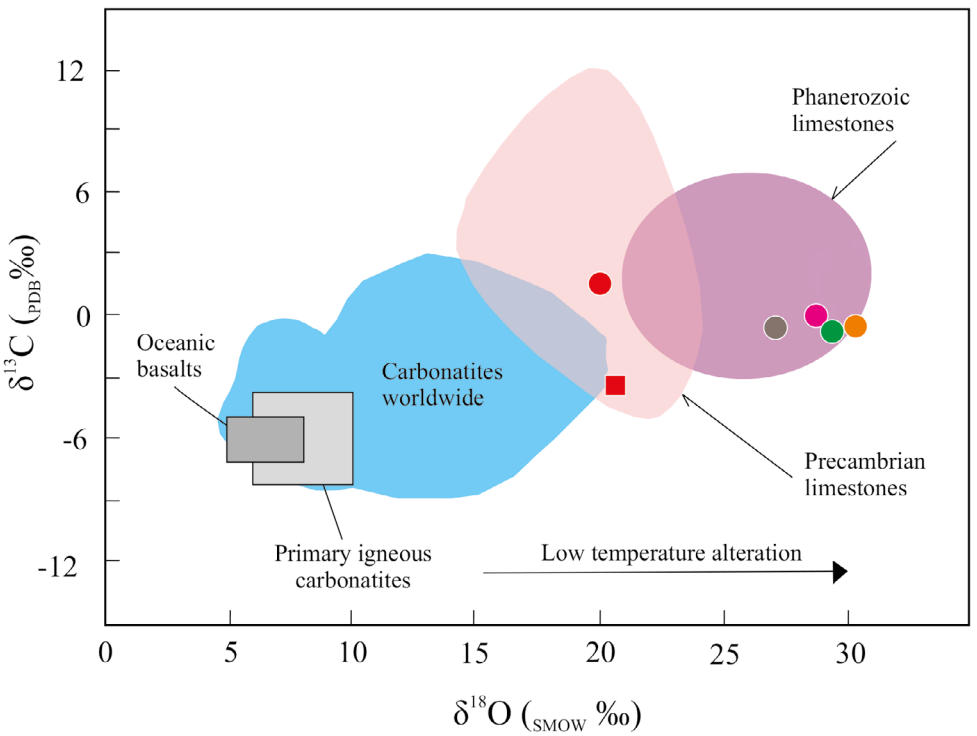

Figure 5. Carbon and oxygen isotopic compositions for carbonate separates from the Eskişehir-Kızılcaören and the Malatya-Kuluncak deposits. Primary igneous carbonatites (PIC) and oceanic basalts boxes are from Deines (1989) and Keller and Hoefs (1995), respectively. Fields for carbonatites from worldwide sources and limestones adapted from Bell and Simonetti (2010). Symbols are the same as in Figure 4.

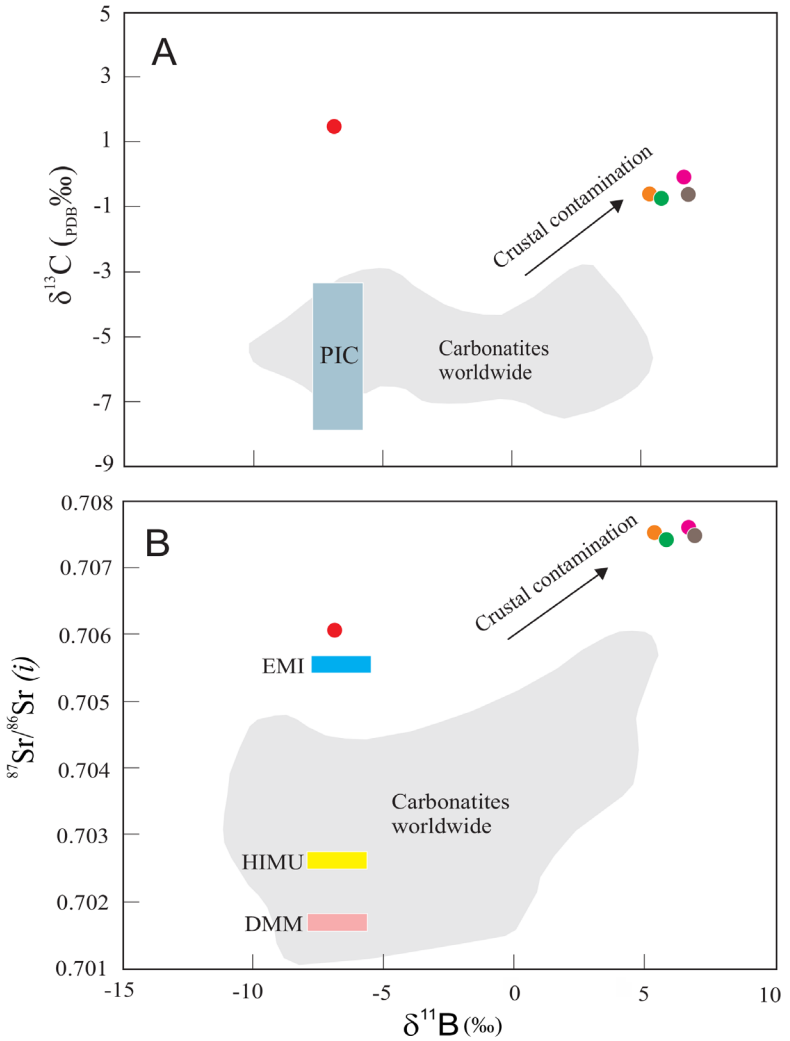

Figure 6. Diagrams of $\delta^{13}C$ **(A)** and initial $^{87}Sr/^{86}Sr(i)$ **(B)** compositions vs $\delta^{11}B$ values for carbonate separates from the the Eskişehir-Kızılcaören and the Malatya-Kuluncak deposits. These are compared (gray field) to those for carbonatite occurrences worldwide (Hulett et al., 2016), the Miaoya complex (Central China, Çimen et al., 2018), and Blue River (British Columbia, Canada), Chipman Lake Carbonatite (Ontario, Canada), Jacupiranga (São Paulo State, Brazil) and Fen complex (Telemark, Norway) regions (Çimen et al., 2019 and references therein). Sr isotope fields for HIMU, EMI and DMM are from Zindler and Hart (1986). Note that asthenospheric $\delta^{11}B$ value of –7.1 ±0.9‰ (Marschall et al., 2017) is attributed to these three mantle components. $\delta^{13}C$ values for PIC are from Deines (1989). Symbols are the same as in Figure 4.

in order to evaluate possible contamination/hydrothermal processes and mantle sources (e.g., Deines, 1989; Keller and Hoefs, 1995). The carbonate rocks from both deposits studied here have much heavier O and C isotope values than primary mantle-derived carbonatites (Figure 5; Keller and Hoefs, 1995), which may have been resulted from low-temperature alteration (e.g., Simonetti et al., 1995), or might be indicative of their sedimentary origin (e.g., Tao et al., 2018). With regards to the carbonate rocks from the Kuluncak deposit, the O and C isotope data reported here confirm their sedimentary origin (Figure 5), whereas the heavier O and C isotope values of the carbonatite sample from the Kızılcaören deposit may be attributed to hydrothermal metasomatism as evidenced by widespread secondary Fe-Mn occurrences in the deposit (e.g., Gültekin et al., 2003).

Recently, Hulett et al. (2016) and Çimen et al. (2018, 2019) have reported that combined boron isotope values with O, C, Sr, Nd, and Pb isotope signatures provide significant insights into mantle source(s) and petrological evolution of carbonatite magmatism. Çimen et al. (2018, 2019) demonstrate that the B isotope system in mantle-derived carbonatite rocks is resistant and not easily affected by later tectono-thermal metamorphic events

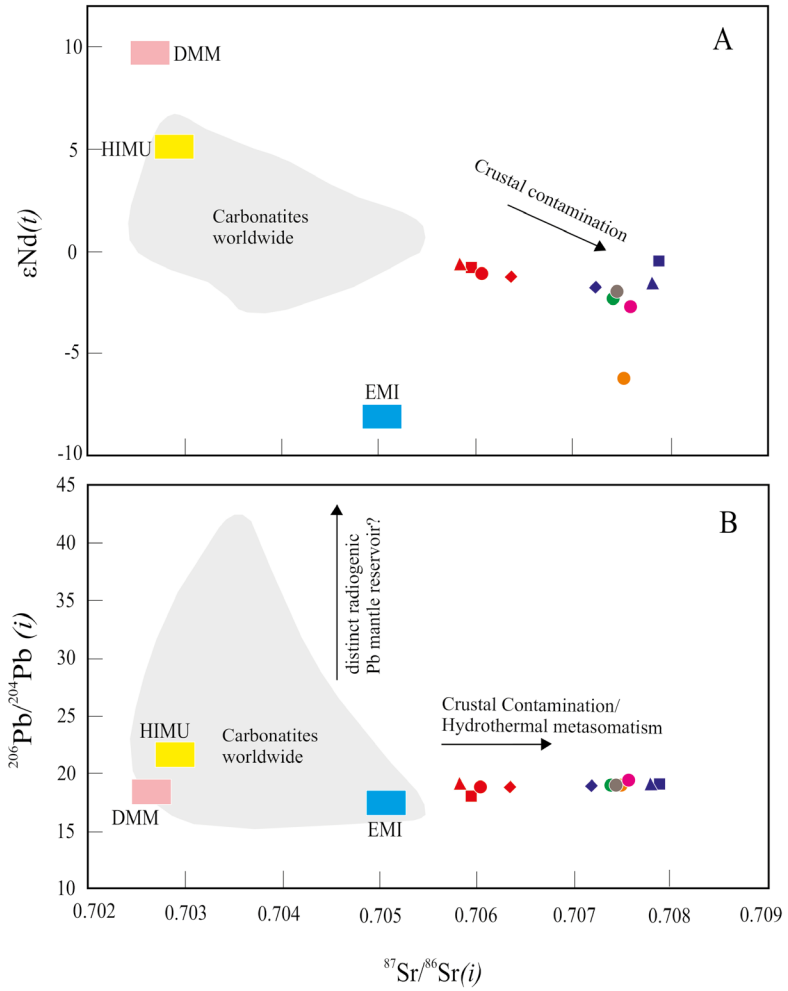

Figure 7. Diagrams of initial $^{87}Sr/^{86}Sr(i)$ compositions vs ε_{Nd} **(A)** and $^{206}Pb/^{204}Pb(i)$ **(B)** values for samples from the Eskişehir-Kızılcaören and the Malatya-Kuluncak deposits. HIMU, EMI and DMM fields are from Zindler and Hart (1986). These are compared (gray field) to those for carbonatite occurrences worldwide (Hulett et al., 2016) and Miaoya complex (Central China, Çimen et al., 2018), and Blue River (British Columbia, Canada), Chipman Lake Carbonatite (Ontario, Canada), Jacupiranga (São Paulo State, Brazil) and Fen complex (Telemark, Norway) regions (Çimen et al., 2019 and references therein). Symbols are the same as in Figure 4.

and late-stage hydrothermal processes. In this study, the B isotope value of –6.83 ±0.5 ‰ for the carbonatite sample from the Kızılcaören deposit is clearly consistent with generation from a typical, asthenospheric-like (MORB) mantle (Figure 6; Marschall et al., 2017), and supports its derivation from an upper mantle source. This is despite the fact that this sample has undergone hydrothermal metasomatic alteration as evidenced by its significantly heavier O and C isotope values compared to primary igneous carbonatites (Table 2, Figure 5). In contrast, the carbonate rocks from the Kuluncak deposit display much heavier B isotope values than MORB mantle (Figure 6), which confirms the sedimentary origin of these carbonates. It has been well established that marine sediments/carbonates are characterized by enriched B isotopes ($\delta^{11}B$ = +2 ‰ to +26 ‰; e.g., Izhikawa and Nakamura, 1993; Kaseman et al., 2009; Paris et al., 2010; De Hoog and Savov, 2018).

The Sr isotope data for the carbonate rocks from both deposits reported here are more radiogenic than those from carbonatites worldwide (Figure 7). While the Sr isotope data for carbonate rocks from the Kuluncak deposit indicate their crustal origin, the slightly more radiogenic Sr isotope value of the carbonatite sample from the Kızılcaören deposit (relative to carbonatites worldwide) could be attributed to hydrothermal metasomatism or contamination from host rocks (i.e. Sr-rich and B-poor contaminant) since its B isotope signature is consistent with mantle-derived carbonatites (Figure 6). The asthenospheric mantle-like B isotope signature

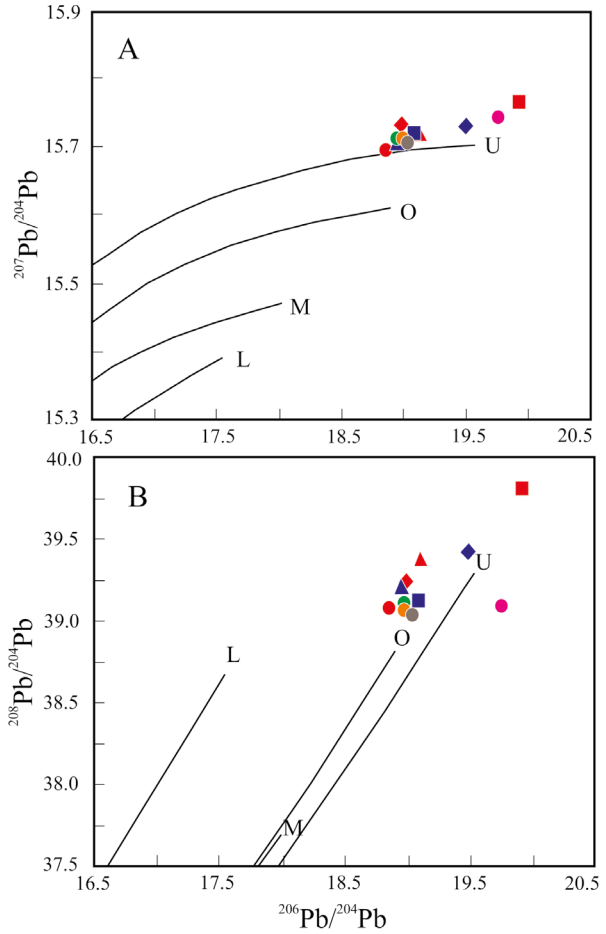

Figure 8. Plots of $^{207}Pb/^{204}Pb$ vs. $^{206}Pb/^{204}Pb$ **(A)** and $^{208}Pb/^{204}Pb$ vs. $^{206}Pb/^{204}Pb$ **(B)** for samples from the Eskişehir-Kızılcaören and the Malatya-Kuluncak deposits. Trends for the upper crust (U), orogenic belt (O), mantle (M) and lower crust (L) are from Zartman and Doe (1981) and Zhou et al. (2016). Symbols are the same as in Figure 4.

for this carbonatite sample rules out both the presence of recycled crustal material in its upper mantle source, or a significant amount of crustal contamination during its petrogenesis. In recent studies, the positive or heavier ($d^{11}B > -7‰$) B isotope values for pristine (i.e. plot within PIC field) carbonatites have been clearly attributed to the involvement of crustal material into their upper mantle source (Hulett et al., 2016; Çimen et al., 2018, 2019). Lastly, the Nd isotope signatures for all samples from both deposits indicate a significant involvement of continental crust (Figure 7A). This interpretation is also confirmed by their $^{207}Pb/^{204}Pb$ and $^{206}Pb/^{204}Pb$ isotope signatures since these plots above the average Pb isotope evolution curve for the upper crust (Figure 8A; Zartman and Doe, 1981). In Figure 8B, the samples mainly fall between the Pb isotope evolution curves for the upper crust and orogenic belts, which may reflect the Alpine orogenic event on the formation of rocks in both regions since Turkey is located in the Mediterranean sector of the Alpine-Himalayan orogenic belt (Göncüoğlu et al., 1997). Here, the Pb-isotope ratio of Tur-2b clearly plots beyond 0-age points of reference curves, which may be attributed to its higher U/Pb ratio (Table 4) compared to the remaining samples.

In summary, the combined chemical, stable, and radiogenic isotope data presented in this study confirm the occurrence of carbonatite-related magmatism in the Kızılcaören deposit, and do not indicate the presence of any mantle-derived carbonatite in the Kuluncak deposit.

6.2. Origin of mineralization and geodynamic constraints

In northwestern Turkey (Figure 1), the Eskişehir-Kızılcaören deposit is associated with the late Oligocene-early Miocene alkaline volcanic rocks (23-26 Ma, K-Ar, and Ar-Ar methods) including phonolite, trachyandesite, and trachyte (Delaloye and Özgenç, 1983; Stumpfl and Kırıkoğlu, 1986; Hatzle, 1992; Gültekin et al., 2003; Sarıfakıoğlu et al., 2009; Nikiforov et al., 2014). In a regional context, following the collision event between the Anatolide-Tauride Terrane and the Sakarya Composite Terrane that lasted from Late Cretaceous to Middle Eocene (Şengör and Yılmaz, 1981; Harris et al., 1994; Okay and Tüysüz, 1999), a widespread calc-alkaline to alkaline magmatism formed in western Anatolia (e.g., Dilek and Altunkaynak, 2007; Ersoy et al., 2012). Here, calc-alkaline magmatism (first magmatic episode) is represented by I-type granitoid and its volcanic equivalents that formed during the early to Late Eocene (54–35 Ma) as a result of slab breakoff-related asthenospheric upwelling and partial melting of the subduction-metasomatized lithospheric mantle (Altunkaynak et al., 2012 and references therein). The second magmatic episode in western Anatolia caused the formation of widespread I-type plutonic and associated volcanic rocks in syn-convergent extensional setting during the Late Oligocene to Middle Miocene (Altunkaynak et al., 2012). Similar to E-W trending faults developed in western Anatolia, in the Eskişehir-Kızılcaören region, the alkaline lavas were injected within local strike-slip faults in this extensional tectonic setting during the Late Oligocene-Early Miocene time, and they may have been generated from an enriched/metasomatized lithospheric mantle source (Sarıfakıoğlu et al., 2009).

There are two different hypotheses proposed for the genesis of the Eskişehir-Kızılcaören deposit; a. REEs formed as a result of hydrothermal mineralization associated with the alkaline volcanism (e.g., Kaplan, 1977; Gültekin et al., 2003). b. Carbonatite magmatism is responsible for the REE mineralization (Daleloye and Özgenç, 1983; Özgenç, 1993, Nikiforov et al., 2014). Moreover, the presence of carbonatite magmatism has

been hotly debated for some time since previous studies did not report combined radiogenic and stable isotope data from the host rocks. As discussed above, the chemical and B isotope data reported here indicate the presence of carbonatite-related magmatism for the Kızılcaören deposit. In addition, the CN-REE patterns and radiogenic isotope data for the carbonatite sample (Tur-1) are similar to those for associated bastnaesite, fluorite, and phonolite samples (Figures 4A and 4C), which may indicate generation from a common mantle source.

In contrast, the Malatya-Kuluncak deposit is located in east-central Turkey (Figure 1) and associated with the Late Cretaceous-Early Paleocene alkaline magmatism (e.g., 65 Ma, K-Ar, Leo et al., 1974; 72-77 Ma, Ar-Ar, Boztuğ et al., 2009; 71 Ma, U-Pb, Kuşcu et al., 2011), which formed in a postcollisional tectonic setting (e.g., Özgenç and İlbeyli, 2009; Kuşcu et al., 2011). In central Anatolia, the Late Cretaceous-Early Paleocene central (e.g., Karaçayır, Davulalan, Hayriye) and east-central (e.g., Murmana, Dumluca, Yellice, Kuluncak) Antolian collisional granioids intrude the central Anatolian ophiolite and metasedimentary units, and overlain by Late Paleocene and younger cover units (Boztuğ et al., 2007). In the Malatya-Kuluncak region, the plutonic rocks represent the eastern part of the Central Anatolian Granitoids (Figure 1), and formed in an extensional setting following the collision of the Tauride-Anatolide Platform with the Central Anatolian Ophiolite and the Eastern Pontides, respectively (Boztuğ et al., 2009). It is suggested that the parental magmas for the alkaline rocks in east-central Anatolia were generated from a subduction-modified mantle source (Kuşcu et al., 2011), and also experienced with crustal assimilation and fractional crystallization processes (Özgenç and İlbeyli, 2009). In relation to the genesis of the Malatya-Kuluncak deposit, a carbonatite-hosted/associated type mineralization has been proposed by several previous studies (Özgenç and Kibici, 1994; Özgenç and İlbeyli, 2009; Öztürk et al., 2019a, b); however, the presence of any carbonatite occurrences in the field have yet to be confirmed or corroborated on the basis of isotope data, field evidence (as dikes, plugs, sills, and lava), or petrographic observations. The combined chemical, stable, and radiogenic isotope data presented in this study, for the first time, indicate that the host rock to the mineralization within the Malatya-Kuluncak deposit consists of hydrothermally metasomatized limestone rather than any mantle-derived carbonatite. Moreover, back-scatter electron images and mineral chemistry data from a mineralized vein clearly reveal that the F-REE-Th phases were transported into the carbonates by Si-rich hydrothermal/magmatic fluids (Figures 3G and 3H).

Overall, for the Kızılcaören deposit, the carbonatite-related mineralization associated with alkaline magmatism could have formed in an extensional tectonic setting during the late Oligocene-early Miocene time. This geodynamic environment is consistent with the typical tectonic setting that hosts a majority of carbonatite complexes worldwide (e.g., East African Rift; Bell and Simonetti, 1996; Oslo Rift in Norway, Goodenough et al., 2018). Contrarily, the mineralization associated with the Late Cretaceous-Early Paleocene alkaline magmatism from the Kuluncak deposit may have been generated in a postcollisional tectonic setting. This deposit may have been formed by a combination of magmatic and hydrothermal processes, as evidenced for similar REE-type deposits worldwide (e.g., Sin Quyen Deposit, Northwestern Vietnam, Li and Zhou, 2018; the Strange Lake deposit in Québec-Labrador, Canada; Williams-Jones et al., 2012 and references therein).

7. Conclusions

The Eskişehir-Kızılcaören and Malatya-Kuluncak deposits represent the most important F-REE-Th mineralizations in Turkey. The combined trace element, stable, and radiogenic isotope data from these regions suggest that the host rocks to the F-REE-Th mineralization consist of hydrothermally metasomatized carbonatite and limestone, respectively. In this study, of particular note is the mantle-like $d^{11}B$ isotope signature, enriched TREE, and low B content for sample Tur-1 (Eskişehir-Kızılcaören region), which support a petrogenetic link to upper mantle-derived carbonatite magmatism. In summary, the REE mineralization associated with the Kızılcaören deposit may be attributed to carbonatite-related magmatism associated with alkaline rocks, whereas the mineralization occurring at the Kuluncak deposit may result from hydrothermal fluids/melts alteration associated with extensive postcollisional magmatism. The latter formed predominantly during contact metasomatism between the plutonic rocks and the limestone in the region. However, future studies should include investigation of additional samples from both deposits to better evaluate the exact origin of the REE-Th-F mineralization.

Acknowledgments

The authors sincerely thank Drs. Ian Steele and Dana Biasatti for EPMA, and O and C isotope analyses, respectively. The University of Notre Dame financially supported this research. O. Çimen acknowledges "The Scientific and Technological Research Council of Turkey (BIDEB-2219 program)" for the postdoctoral scholarship. In addition, Dr. Yalçın Ersoy is thanked for providing the samples from the Eskişehir-Kızılcaören region. We also acknowledge Dr. Gültekin Topuz (Topic Editor) and anonymous reviewer for their constructive comments, which have resulted in an improved manuscript.

References

Altunkaynak S, Dilek Y, Genc CS, Sunal G, Gertisser R et al. (2012) Spatial, temporal and geochemical evolution of Oligo–Miocene granitoid magmatism in western Anatolia, Turkey. Gondwana Research 21: 961-986.

Bell K, Simonetti A (1996). Carbonatite magmatism and plume activity: implications from the Nd, Pb and Sr isotope systematics of Oldoinyo Lengai. Journal of Petrology 37: 1321-1339.

Bell K, Simonetti A (2010). Source of parental melts to carbonatites–critical isotopic constraints. Mineralogy and Petrology 98: 77-89.

Boztuğ D, Harlavan Y, Arehart GB, Satır M, Avci N (2007). K-Ar age, whole-rock and isotope geochemistry of A-type granitoids in the Divriği-Sivas region, easterncentral Anatolia, Turkey. Lithos 97: 193-218.

Boztuğ D, Jonckheere RC, Heizler M, Ratschbacher L, Harlavan Y et al. (2009). Timing of post-obduction granitoids from intrusion through cooling to exhumation in central Anatolia, Turkey. Tectonophysics 473:223-233.

Chakhmouradian AR, Wall F (2012). Rare earth elements: minerals, mines, magnets (and more). Elements 8, 333-340.

Çimen O, Göncüoğlu MC, Simonetti A, Sayit K (2017). Whole rock geochemistry, zircon U-Pb and Hf isotope systematics of the Çangaldağ pluton: evidences for middle jurassic continental arc magmatism in the Central Pontides, Turkey. Lithos 288-289C: 35-54.

Çimen O, Kuebler C, Monaco B, Simonetti SS, Corcoran L et al. (2018). Boron, Carbon, Oxygen and Radiogenic Isotope Investigation of Carbonatite from the Miaoya complex, central China: Evidences for late-stage REE hydrothermal event and mantle source heterogeneity. Lithos 322: 225-237.

Çimen O, Kuebler C, Simonetti SS, Corcoran L, Mitchell R et al. (2019). Combined Boron, Radiogenic (Nd, Pb, Sr), Stable (C, O) Isotopic and Geochemical Investigations of Carbonatites From the Blue River Region, British Columbia (Canada): Implications for Mantle Sources and Recycling of Crustal Carbon. Chemical Geology 529: 119240.

Chen W, Liu H-Y, Lu J, Jiang S-Y, Simonetti A et al. (2019). The formation of the ore-bearing dolomite from the giant Bayan Obo REE-Nb-Fe deposit, Inner Mongolia: Insights from micron-scale geochemical data. Mineralium Deposita. doi: 10.1007/s00126-019-00886-4

De Hoog JCM, Savov IP (2018). Boron Isotopes as a Tracer of Subduction Zone Processes. In: Marschall H., Foster G. (eds) Boron Isotopes. Advances in Isotope Geochemistry. Springer, Cham. doi: 10.1007/978-3-319-64666-4_9.

Delaloye M, Özgenç İ (1983). Petrography and age determinations of the alkaline volcanic rocks and carbonatite of Kızılcaören district, Beylikahır-Eskişehir, Turkey. Schweizerische mineralogische und petrographische Mitteilungen 63: 289-294.

Deines P (1989). Stable Isotope Variations in Carbonatites: Carbonatites: Genesis and Evolution. 13, Unwin Hyman.

Dilek Y, Altunkaynak S (2007). Cenozoic crustal evolution and mantle dynamics of post-collisional magmatism in western Anatolia. International Geology Review 49 (5): 431-453.

Ersoy YE, Helvacı C, Uysal İ, Karaoğlu Ö, Palmer MR et al. (2012). Petrogenesis of the Miocene volcanism along the İzmir-Balıkesir Transfer Zone in western Anatolia, Turkey: Implications for origin and evolution of potassic volcanism in post-collisional areas. Journal of Volcanology and Geothermal Research 241-242: 21-38.

Ersoy EY, Uysal I, Gündoğan I (2018). Association of Alkaline Silicate and Carbonatite Rocks in Kızılcaören (Eskişehir) District: Implications for Liquid Immiscibility Processes in Genesis of Carbonatite Magmatism. 8. Geochemistry Symposium. Abstract Book. p.86.

Fu W, Luo P, Hu Z, Feng Y, Liu L et al. (2019). Enrichment of ion-exchangeable rare earth elements by felsic volcanic rock weathering in South China: Genetic mechanism and formation preference. Ore Geology Reviews 114: 103120.

Goodenough KM, Schilling J, Jonsson E, Kalvig P, Charles N et al. (2016). Europe's rare earth element resource potential: an overview of REE metallogenetic provinces and their geodynamic setting. Ore Geology Reviews 72: 838-856.

Göncüoğlu MC, Kozlu H, Dirik K (1997). Pre-alpine and alpine terranes in Turkey: explanatory notes to the terrane map of Turkey. Annales Géologiques des Pays Helléniques 37: 515-536.

Gültekin AH, Örgün Y, Suner F (2003). Geology, mineralogy and fluid inclusion data of the Kizilcaoren fluorite- barite- REE deposit, Eskisehir, Turkey. Journal of Asian Earth Sciences 21: 365-376.

Harris NBW, Kelley S, Okay AI (1994). Post-collisional magmatism and tectonics in northwest Anatolia. Contributions to Mineralogy and Petrology 117: 241-252.

Hatzle T (1992). Die Genese Der Karbonatit-und Alkalivulkanit-Assoziierten Fluorit-Baryt-Bastnasit-Vererzung Bei Kızılcaören (Turkei). Münchner Geol. Hefte. Technischen Universitat München: 271 pp (in German).

Hoernle K, Tilton G, Le Bas MJ, Duggen S, Garbe-Schönberg D (2002). Geochemistry of oceanic carbonatites compared with continental carbonatites; mantle recycling of oceanic crustal carbonate. Contributions to Mineralogy and Petrology 142: 520-542.

Hulett SRW, Simonetti A, Rasbury ET, Hemming NG (2016). Recycling of subducted crustal components into carbonatite melts revealed by boron isotopes. Nature Geoscience 9: 904-908.

Ishikawa T, Nakamura E (1993). Boron isotope systematics of marine sediments. Earth and Planetary Science Letters 117: 567-580.

Jaireth S, Hoatson DM, Miezitis Y (2014). Geological setting and resources of the major rare-earth-element deposits in Australia. Ore Geology Reviews 62: 72-128.

Jones AP, Genge M, Carmody L (2013). Carbonate melts and carbonatites. Reviews in Mineralogy and Geochemistry 75: 289-322.

Jordens A, Cheng YP, Waters KE (2013). A review of the beneficiation of rare earth element bearing minerals. Minerals Engineering 41: 97-114.

Kaplan H (1977). Rare earth elements and thorium complex deposit of Kizilcaören village, Sivrihisar-Eskişehir, Turkey. Bulletin of Geological Engineering 2: 69-76.

Kasemann SA, Schmidt DN, Bijma J, Foster GV (2009). In situ boron isotope analysis in marine carbonates and its application for foraminifera and palaeo-Ph. Chemical Geology 260 (1-2): 138-147.

Keller J, Hoefs J (1995). Stable Isotope Characteristics of Recent Natrocarbonatites from Oldoinyo Lengai. Carbonatite Volcanism, IAVCEI Proceedings in Volcanology 4: 113-123.

Kogarko LN, Sorokhtina NV, Zaitsev VA, Senin VG (2009). Rare Metal Mineralization of Calcite Carbonatites from the Cape Verde Archipelago. Geochemistry International 47: 531-549.

Kuşcu İ, Yılmazer E, Güleç NT, Bayır S, Demirela G et al. (2011). U Pb and ^{40}Ar-^{39}Ar geochronology and isotopic constraints on the genesis of copper gold bearing iron oxide deposits in the Hasançelebi district eastern Turkey. Economic Geology 106: 261-288.

Kynicky J, Smith MP, Xu C (2012). Diversity of rare earth deposits: the key example of China. Elements 8: 361-367.

Leo GW, Marvin RF, Mehnert HH (1974). Geological framework of Kuluncak–Sofular area, east-central Turkey, and K-Ar ages of igneous rocks. Geological Society of America Bulletin 85: 1785-1788.

Leo WG, Önder E, Kılıç M, Avcı M (1978). Geology and mineral resources of Kuluncak-Sofular area (Malatya K39-a1-K39-a2 quadrangles), Turkey. U.S. Geol Survey Bullettin pp. 1429.

Li XC, Zhou MF (2018). The Nature and Origin of Hydrothermal REE Mineralization in the Sin Quyen Deposit, Northwestern Vietnam. Economic Geology 113 (3): 645-673.

Marschall HR, Wanles VD, Shimizu N, Pogge Von Strandmann PAE, Elliott T et al. (2017). The boron and lithium isotopic composition of mid-ocean ridge basalts and the mantle. Geochimica et Cosmochimica Acta 207: 102-138.

McDonough WF, Sun SS (1995). The composition of the Earth. Chemical Geology 120: 223-253.

Millonig LJ, Gerdes A, Groat LA (2012). U-Th-Pb geochronology of meta-carbonatites and meta-alkaline rocks in the southern Canadian Cordillera: a geodynamic perspective. Lithos 152: 202-217.

Mitchell R, Chudy T, McFarlane CRM, Wu FY (2017). Trace element and isotopic composition of apatite in carbonatites from the Blue River area (British Columbia, Canada) and mineralogy of associated silicate rocks. Lithos 286-287: 75-91.

MTA Genel Müdürlüğü (2017). Dünyada ve Türkiye'de Nadir Toprak Elementleri, Fizibilite Etütleri Daire Başkanlığı (In Turkish).

Nikiforov AV, Öztürk H, Altuncu S, Lebedev VA (2014). Kizilcaören Ore-bearing Complex with Carbonatites (Northwestern Anatolia, Turkey): Formation Time and Mineralogy of Rocks. Geology of Ore Deposits 56: 35-60.

Okay AI, Tüysüz O (1999). Tethyan sutures of Northern Turkey. In: Durand B, Jolivet L, Horthváth F, Séranne M (Eds.). The Mediterranean Basin: Tertiary Extension within the Alpine Orogen. Geological Society, London, Special Publication 156: 475-515.

Okay AI, Göncüoğlu MC (2004). Karakaya Complex: a review of data and concepts. Turkish Journal of Earth Sciences 13: 77-95.

Özgenç İ (1993). Geology and REE-geochemistry of carbothermal bastnaesite–fluorite–barite deposit of Kızılcaören (Sivrihisar, Eskişehir), Geological Bulletin of Turkey 36: 1-11.

Özgenç İ, Kibici Y (1994). The geology and chemical-mineralogical properties of Britholite veins of Başören village (Kuluncak-Malatya). Geological Bulletin of Turkey 37: 77-85.

Özgenç İ, İlbeyli N (2009). Geochemical constraints on petrogenesis of Late Cretaceous alkaline magmatism in east-central Anatolia (Hasancelebi–Basören, Malatya), Turkey. Mineralogy and Petrology 95: 71-85.

Öztürk H, Altuncu S, Hanilçi N, Kasapçı C, Goodenough KM (2019a). Rare earth element-bearing fluorite deposits of Turkey: An overview. Ore Geology Reviews 105: 423-444.

Öztürk H, Hanilçi N, Altuncu S, Kasapçı C (2019b). Rare earth element (REE) resources of Turkey: An overview of their characteristics and origin. Bulletin of the Mineral Research and Exploration 159: 129-143.

Paris G, Bartolini A, Donnadieu Y, Beaumont V, Gaillardet J (2010). Investigating boron isotopes in a middle Jurassic micritic sequence: Primary vs. diagenetic signal. Chemical Geology 275 (3-4): 117-126.

Sarıfakıoğlu E, Özen H, Hall C (2009). Petrogenesis of extension-related alkaline volcanism in Karaburhan (Sivrihisar–Eskisehir), NW Anatolia, Turkey. Journal of Asian Earth Science 35: 502-515.

Sayit K, Göncüoğlu MC (2009). Geochemistry of mafic rocks of the Karakaya complex, Turkey: evidence for plume-involvement in the Palaeotethyan extensional regime during the Middle and Late Triassic. International Journal of Earth Sciences 98: 157-185.

Simonetti A, Bell K (1993). Isotopic disequilibrium in clinopyroxenes from nephelinitic lavas, Napak volcano, eastern Uganda. Geology 21: 243-246.

Simonetti A, Bell K, Viladkar SG (1995). Isotopic data from the Amba Dongar Carbonatite Complex, west-central India: Evidence for an enriched mantle source. Chemical Geology 122: 185-198.

Spivack AJ, Edmond JM (1987). Boron isotope exchange between seawater and the oceanic crust. Geochimica et Cosmochimica Acta 51: 1033-1043.

Stumpfl EF, Kırıkoğlu MS (1986). Fluorite–barite–rare earth deposit at Kızılcaören, Turkey, Mitteilungen der Österreichischen Geographischen Gesellschaft 78: 193-200.

Şengör AMC, Yılmaz Y (1981). Tethyan evolution of Turkey: a plate tectonic approach. Tectonophysics 75: 181-241.

Tao R, Zhang L, Li S, Zhu J, Ke S (2018). Significant contrast in the Mg-C-O isotopes of carbonate between carbonated eclogite and marble from the S.W. Tianshan UHP subduction zone: Evidence for two sources of recycled carbon. Chemical Geology 483: 65-77.

Verplank PL (2017). The role of fluids in the formation of rare earth element deposits. Procedia Earth and Planetary Science 17: 758-761.

Walters AS, Goodenough KM, Hughes HSR, Roberts NMW, Gunn AG et al. (2013). Enrichment of rare earth elements during magmatic and post-magmatic processes: a case study from the loch loyal syenite complex, northern Scotland. Contributions to Mineralogy and Petrology 166: 1177-1202.

Williams-Jones AE, Migdisov AA, Samson IM (2012). Hydrothermal mobilisation of the rare earth elements - a tale of "ceria" and "yttria". Elements 8: 355-360.

Woolley AR (1989). The Spatial and Temporal Distribution of Carbonatites: Carbonatites: Genesis and Evolution. Unwin Hyman 15-37.

Woolley AR, Kempe DRC (1989). Carbonatites: nomenclature, average chemical compositions, and element distribution. In: Bell, K. (ed.) Carbonatites: Genesis and Evolution. Unwin Hyman, London, p. 1-13.

Wunder B, Meixner A, Romer RL, Wirth R, Heinrich W (2005). The geochemical cycle of boron: constraints from boron isotope partitioning experiments between mica and fluid. Lithos 84: 206-216.

Xu C, Wang L, Song W, Wu M (2010). Carbonatites in China: A review for genesis and mineralization. Geoscience Frontiers 1: 105-114.

Yang, X.J., Lin, A., Li, X.L., Wu, Y., Zhou, W et al. (2013). China's ion-adsorpsion rare earth resources, mining consequences and preservation. Environmental Development 8: 131-136.

Zartman RE, Doe BR (1981). Plumbotectonics—the model. Tectonophysics 75: 135-162.

Zhang SH, Zhao Y, Liu Y (2017). A precise zircon Th-Pb age of carbonatite sills from the world's largest Bayan Obo deposit: Implications for timing and genesis of REE-Nb mineralization. Precambrian Research 291: 202-219.

Zheng X, Lui Y (2019). Mechanisms of element precipitation in carbonatite-related rare-earth element deposits: Evidence from fluid inclusions in the Maoniuping deposit, Sichuan Province, southwestern China. Ore Geology Reviews 107: 218-238.

Zhou JX, Luo K, Li B, Huang ZL, Yan ZF (2016). Geological and isotopic constraints on the origin of the Anle carbonate-hosted Zn–Pb deposit in northwestern Yunnan Province, SW China. Ore Geology Reviews 74: 88-100.

Zindler A, Hart SR (1986). Chemical dynamics. Annual Review of Earth And Planetary Sciences 14: 493-571.